

ARTICLE OPEN



Balancing efficiency and transparency in organic transparent photovoltaics

Ruiqian Meng^{1,2,3}, Qianqing Jiang^{2,3} and Dianyi Liu^{1,2,3}

The challenges in transparent photovoltaic (TPV) fields are still that the device transparency and efficiency are difficult to be balanced to meet the requirements of practical applications. In this study, we systematically investigated the interrelationship between photovoltaic film properties, optical transmission, and photovoltaic performances in the near-infrared harvesting organic TPVs. The results indicate that the photovoltaic film thickness determines the TPV's transparency and meanwhile affects the device efficiency; by contrast, the donor–acceptor ratio only affects device efficiency and has little effect on transparency. By controlling the film thickness and donor–acceptor ratio, the average visible transmission (AVT) of TPVs can be precisely managed in the range of 40%–85%, and the device efficiency can achieve as high as 4.06% and 2.38% while the AVT exceeds 70% and 80%, respectively. Importantly, the large area (~10 cm²) TPV modules and ultra-flexible devices were then successfully prepared based on the systematical study.

npj Flexible Electronics (2022)6:39; <https://doi.org/10.1038/s41528-022-00173-9>

INTRODUCTION

Compared with opaque photovoltaics, transparent photovoltaic (TPV) techniques can not only convert solar energy into electricity but also provide a natural visible-light environment, which offers a special way to utilize solar energy^{1–3}. The high-transparency property enables the broader application occasions of TPVs, for example, when the average visible transmission (AVT) achieves over 70%, the TPVs will meet the transmission requirements to use on office or living room windows². Some special applications will also be available under highly transparent conditions, such as the invisible self-powered wearable devices. The performance of the TPVs with AVT < 70% has been improved fast under the efforts of researchers. Particularly, the power conversion efficiencies (PCE) of the TPVs with the AVT exceeding 50% have already been promoted to about 10% in both single-junction and tandem transparent solar cells^{4–6}. However, the challenges in TPV fields still exist clearly: (1) the AVT is difficult to exceed 80%, as a result, it is difficult to meet the application function and aesthetic requirements; (2) with the increase in device transparency, the efficiency of the device drops quickly, therefore the transparency and efficiency are difficult to be balanced in highly transparent TPVs.

The key strategy to develop highly transparent TPVs is adopting invisible-light (ultraviolet and near-infrared light) absorption semiconductors. In previous reports, the AVTs of TPV devices based on ultraviolet (UV) selective harvesting semiconductors can be easily obtained over 70%^{7–10}. Unfortunately, because the number of UV photons is limited and the theoretical efficiency is less than 7%¹¹, the efficiencies of UV-selective TPVs are still restricted at ~1% level until now. Since over half of the solar energy is distributed within the near-infrared (NIR) region, the TPVs with NIR-harvesting semiconductors are expected to achieve higher efficiency than the TPVs with UV-selective materials. Plenty of efforts are paid to the development of organic dyes with strong NIR-harvesting capability in TPVs^{3,12–14}. Though the devices

display the expected high transparency, the efficiencies are still limited. To further enhance the efficiency, some devices have to work with the liquid electrolyte¹², which might limit its applications.

In order to meet more application requirements, exploring the solid-state TPV devices and further improving device performance by well-balancing the transparency and efficiency are the essential research goals for the next studies. Here, we take the reported NIR-harvesting organic semiconductors as an example to show how to balance the efficiency and transparency in TPVs. By adopting the highly transparent electrodes, we demonstrate the highly transparent TPVs with the AVTs exceeding 80%. How the ratios of donor–acceptor, the thicknesses of the active layer affect the device optical transmission and photovoltaic performance is systematically investigated and discussed. The results indicate that the photovoltaic film thickness determines the TPV's transparency and meanwhile affects the device efficiency; by contrast, the D–A ratio only affects the efficiency and has little effect on device transparency. According to the results, we can precisely tune the AVT of TPVs from 40% to over 80%, the PCE can be achieved as high as 4.06% and 2.38% while the device AVT exceeds 70% and 80%, respectively. By adopting the laser-patterning techniques, the large area TPV modules (~10 cm²) are successfully prepared on rigid substrates. The ultra-flexible TPV modules are also successfully fabricated in this work. The study presents a good reference to design the self-powered and invisible applications prepared with the highly transparent TPVs.

RESULTS AND DISCUSSION

The development of the highly transparent and efficient TPVs strongly relies on the specific transparent materials, and the semiconductors are among the key materials. Organic photovoltaic semiconductors with NIR-harvesting capability are the promising materials for the development of TPVs^{15,16}. Some

¹Zhejiang University, Hangzhou 310013 Zhejiang Province, China. ²Key Laboratory of 3D Micro/Nano Fabrication and Characterization of Zhejiang Province, Research Center for Industries of the Future and School of Engineering, Westlake University, 18 Shilongshan Road, Hangzhou 310024 Zhejiang Province, China. ³Institute of Advanced Technology, Westlake Institute for Advanced Study, 18 Shilongshan Road, Hangzhou 310024 Zhejiang Province, China. ✉email: jiangqianqing@westlake.edu.cn; liudianyi@westlake.edu.cn

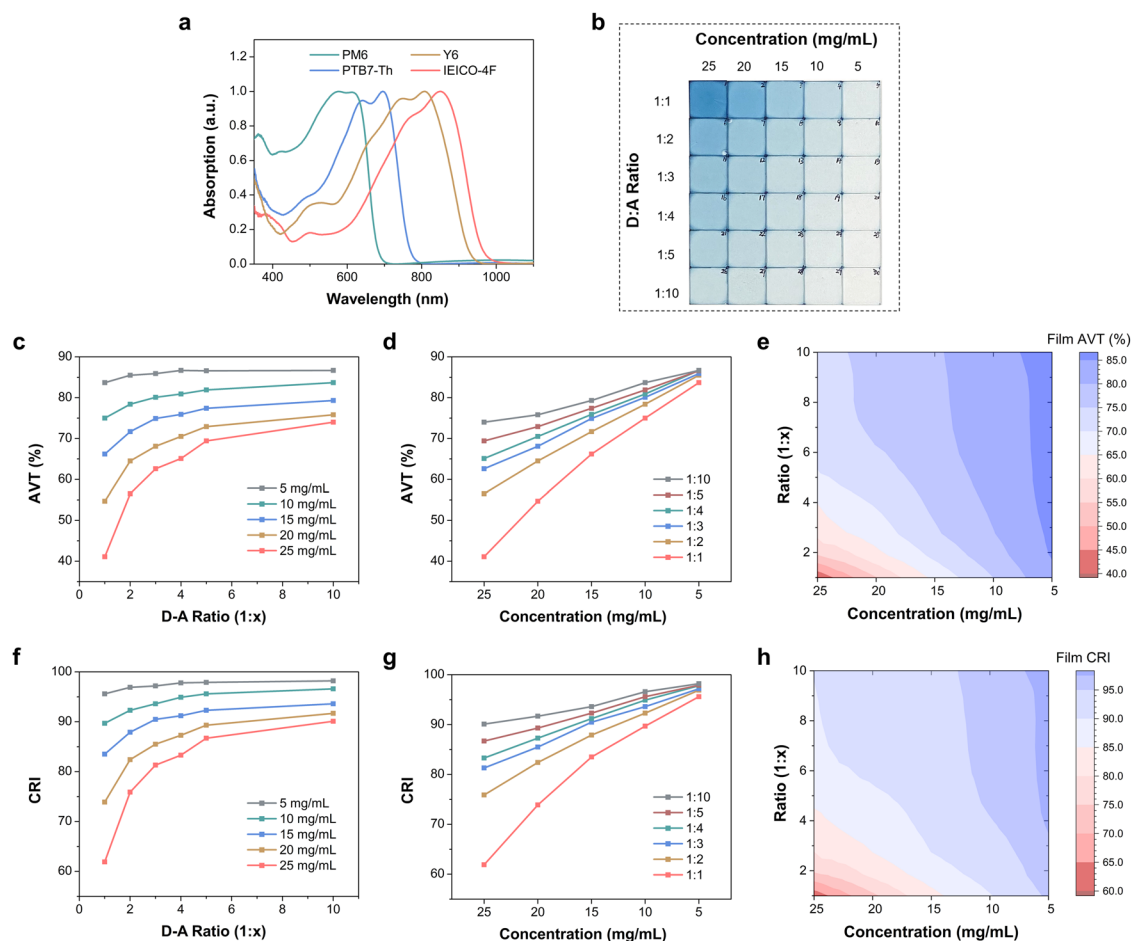


Fig. 1 Film optical properties. **a** Absorption spectra of the different donor and acceptor films. **b** Photograph of BJJ films which prepared with various D–A ratios or precursor concentrations on the glass substrate. **c–h** AVT, CRI values and models of the BJJ films prepared with various D–A ratios or precursor concentrations.

efficient emerging organic semiconductors with NIR-harvesting capability are introduced in semitransparent solar cells recently and present good device performance^{6,17–20}. For example, PM6:Y6 as one of the famous donor/acceptor pairs enables the PCE and AVT of semitransparent devices to achieve 12.37% and 18.6%, respectively (Supplementary Fig. 1)^{21,22}. However, considering the strong absorption in the visible-light region (Fig. 1a), especially for the donor PM6, the PM6:Y6 pair is not the ideal candidate for developing highly transparent TPVs. The donor PTB7-Th and the acceptor IEICO-4F are selected as the example active layer materials to introduce the exploration of the highly transparent TPVs in this study (Supplementary Fig. 1). Because of the low visible-light absorption and the satisfied photovoltaic performance²³, the PTB7-Th:IEICO-4F blend film has been broadly used to develop semitransparent solar cells^{6,17,24}. The balancing systems including simulation and experiments based on this blend film are already been attempted in semitransparent solar cells (AVT < 50%)¹⁷. In spite of the high efficiencies, the devices only show the AVTs of less than 40% in previous reports. The low transparency indicates again the difficulty of balancing the photovoltaic performance and device transparency. The lack of highly transparent electrodes is also be suspected as an important reason for the low device transparency. To better understand the influence factors, and further expand the basic knowledge of the balancing process in highly transparent TPVs (AVT > 50%), a systematic study is designed and conducted. Here, we take the reported PTB7-Th:IEICO-4F donor–acceptor (D–A) pair as an

example to show how to balance the efficiency and transparency in TPVs.

Balancing efficiency and transparency

Reducing the content of the visible-light-harvesting semiconductor is proved an effective method to enhance the TPV transparency in semitransparent solar cells^{5,24,25}. With the ultra-narrow bandgap (1.24 eV)²⁶, IEICO-4F can only slightly absorb the red light (600–650 nm), which indicates a good transparent semiconductor candidate for TPV. By contrast, PTB7-Th shows a part of absorption in the visible region of 550–650 nm²⁷. Reducing the use amount of PTB7-Th in the active layer is expected to enhance the transparency of the TPVs²⁴. Applying thinner films is also a useful approach to restrict the absorption in the visible region (Supplementary Fig. 2, Supplementary Table 1)⁸. Thus, to evaluate the influence of the visible-light absorption on the optical performance of photovoltaic BJJ films and TPVs, two approaches are adopted to adjust the BJJ-film absorption properties in the study: (1) varying the D–A ratio in the BJJ blend film; (2) changing the thickness of the active layer.

The precursor solutions are prepared with various D–A ratios and concentrations, and subsequently spin-coated on the bare glass substrates to form the BJJ films (Fig. 1b). The film transmission spectra are drawn in Supplementary Figs. 3, 4, respectively. We take the [D–A ratio = 1:1] and [15 mg/mL] precursor samples as examples for discussion. Supplementary Figure 3c shows that the film's transmission spectra in the region

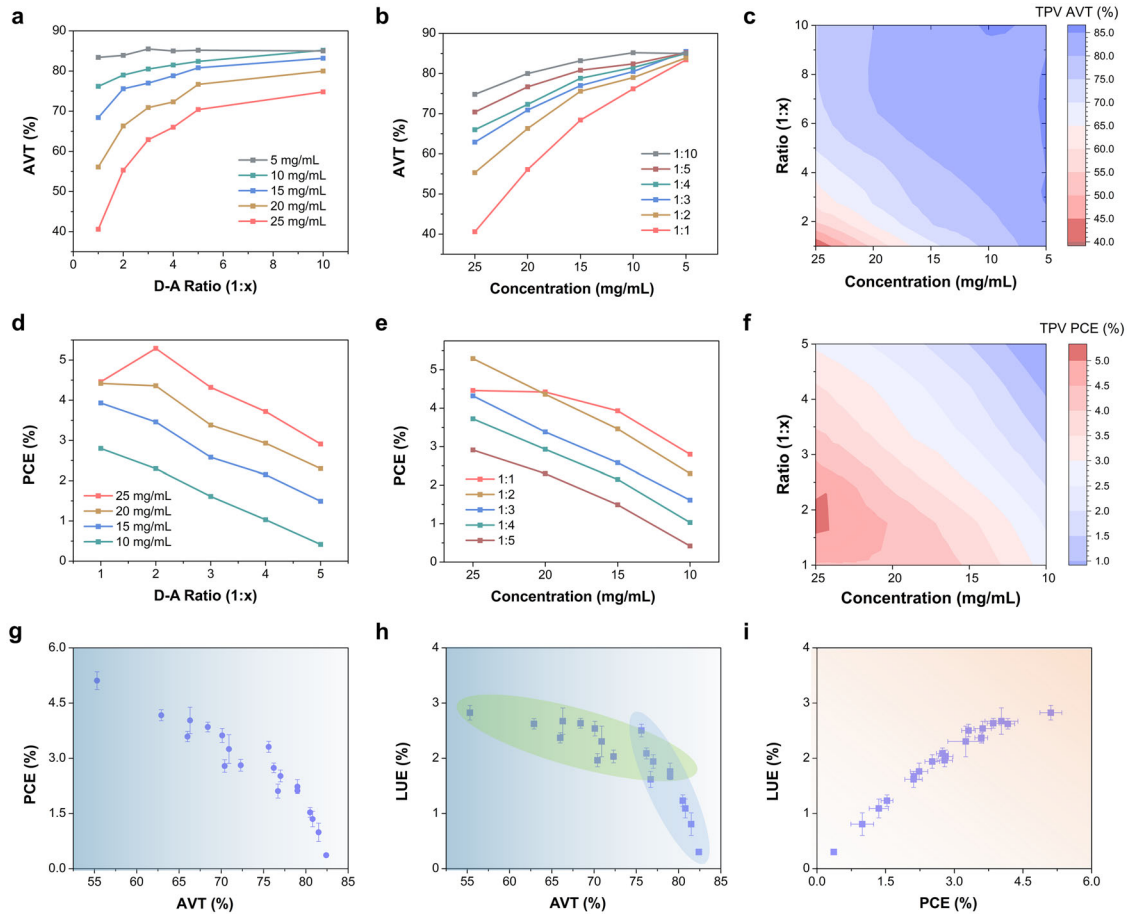


Fig. 2 TPV optical properties and photovoltaic performances. AVT (a–c), PCE (d–f) plots and models of the TPV devices prepared with various D–A ratios or precursor concentrations. (g–i) Relationships between PCE, LUE and AVT in prepared TPVs. Error bars represent the standard deviation.

Table 1. Summarization of AVT and PCE in active layer films and TPVs.

D–A ratio	AVT (%) and PCE (%) with various precursor concentrations					
		25 mg/mL	20 mg/mL	15 mg/mL	10 mg/mL	5 mg/mL
1:1	AVT _{Film}	41.1	54.7	66.2	75.0	83.7
	AVT _{TPV}	40.6	56.1	68.4	76.2	83.4
	PCE _{TPV}	4.46	4.42	3.93	2.80	–
1:2	AVT _{Film}	56.5	64.5	71.7	78.4	85.5
	AVT _{TPV}	55.3	66.3	75.6	79.0	83.9
	PCE _{TPV}	5.29	4.36	3.46	2.30	–
1:3	AVT _{Film}	62.6	68.1	74.9	80.1	85.9
	AVT _{TPV}	62.9	70.9	77.0	80.5	85.5
	PCE _{TPV}	4.32	3.38	2.58	1.61	–
1:4	AVT _{Film}	65.1	70.5	75.9	80.9	86.7
	AVT _{TPV}	66.0	72.3	78.8	81.5	85.0
	PCE _{TPV}	3.72	2.93	2.15	1.03	–
1:5	AVT _{Film}	69.4	72.9	77.4	81.9	86.6
	AVT _{TPV}	70.4	76.7	80.8	82.4	85.2
	PCE _{TPV}	2.91	2.30	1.49	0.417	–
1:10	AVT _{Film}	74.0	75.8	79.3	83.7	86.7
	AVT _{TPV}	74.8	80.0	83.2	85.2	85.0
	PCE _{TPV}	–	–	–	–	–

of 350–750 nm changed dramatically along with the variation of D–A ratio, while the transmission at the NIR region did not change significantly. When the D–A ratio changes from 1:1 to 1:10, the visible-light absorption from PTB7-Th is dramatically weakened, resulting in the film transmission increases obviously, and the AVT of the film correspondingly increased from 41.1% to 74.0%. The corresponding optical parameters including AVT and the color rendering index (CRI) are summarized and plotted as the function of D–A ratios and precursor concentrations to describe the optical property of the as-prepared transparent films (Fig. 1c–h, Supplementary Tables 2, 3).

The film thicknesses and concentration of precursor solutions are listed in Supplementary Table 4. For [D–A ratio = 1:1] set of films, when the film thickness decreases from 157 nm to 14 nm, the film transmission increases obviously throughout the entire spectrum range, and the AVT of the film accordingly increased from 41.1% to 83.7%. To further evaluate the impact of film transmission by precursor condition, we performed the modeling of the film AVT and CRI which was determined by precursor conditions including D–A ratio and precursor concentration (Fig. 1e, h). The modeling results clearly show the zones with various optical parameter values, and it helps guide the preparation of transparent photovoltaic films. Because the active layer is the

main light absorption source in organic-based TPVs which is one of the key influences for the device transparency as well, the results provide a basic reference to guide the preparation of highly transparent TPVs. However, the film is hard to achieve the AVT > 90% even though the film thickness is less than 10 nm since the reflection and light absorption always exist for the films and substrates.

After the systematical studies on the transparent photovoltaic films, the TPV devices are subsequently prepared based on the above organic BHJ films. Two series of TPVs with different device architecture and top transparent electrodes are fabricated respectively. The highly transparent Ag NWs film and the polymer-based PH1000 are used as the top transparent electrode for the normal and inverted structured device, respectively (Supplementary Figs. 5, 6 and Supplementary Table 5)^{28–30}. We take the Ag NWs-based TPV as an example to discuss the device's performance. The Glass/ITO is used as the substrate and bottom transparent electrode, and the architecture of ITO/PEDOT/PTB7-Th:IEICO-4F/ZnO/Ag NWs is adopted for the TPVs (Fig. 3a). The pulsed laser is used to pattern the top-electrode and finally determine the device area²⁸. The transmission spectra of TPVs are also measured according to the related transparent photovoltaic films (Supplementary Figs. 7, 8), and the corresponding optical parameters are

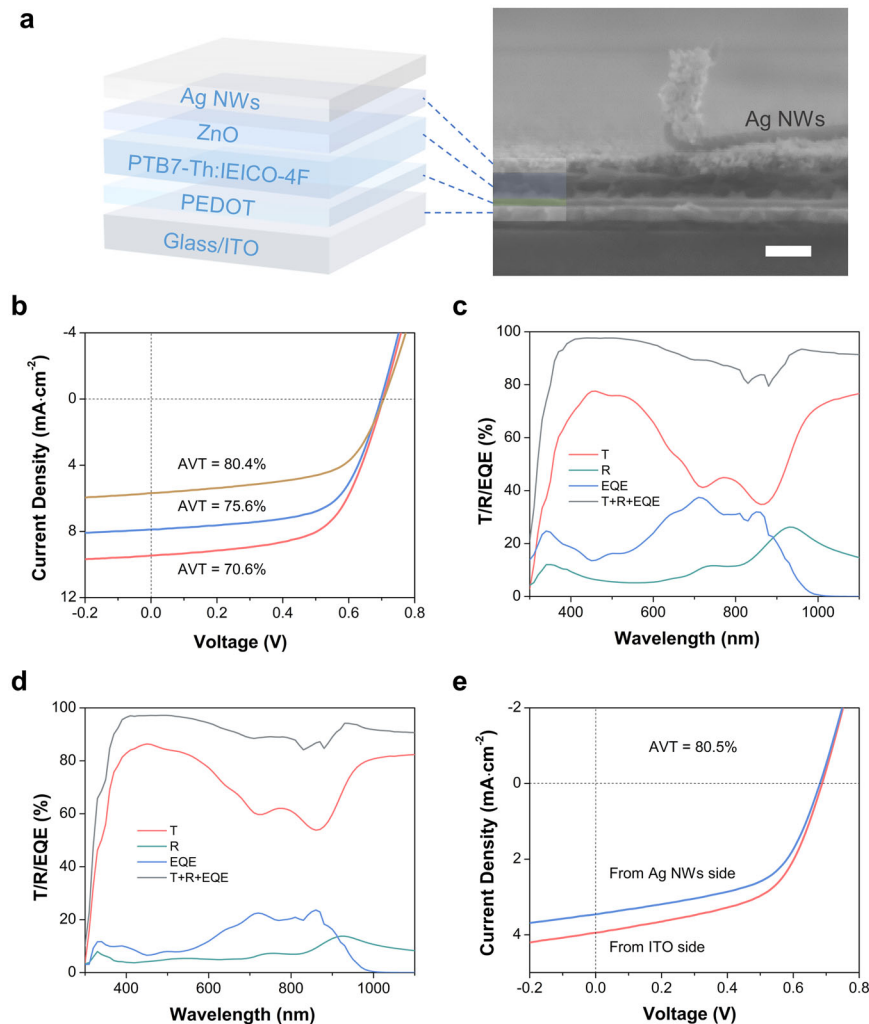
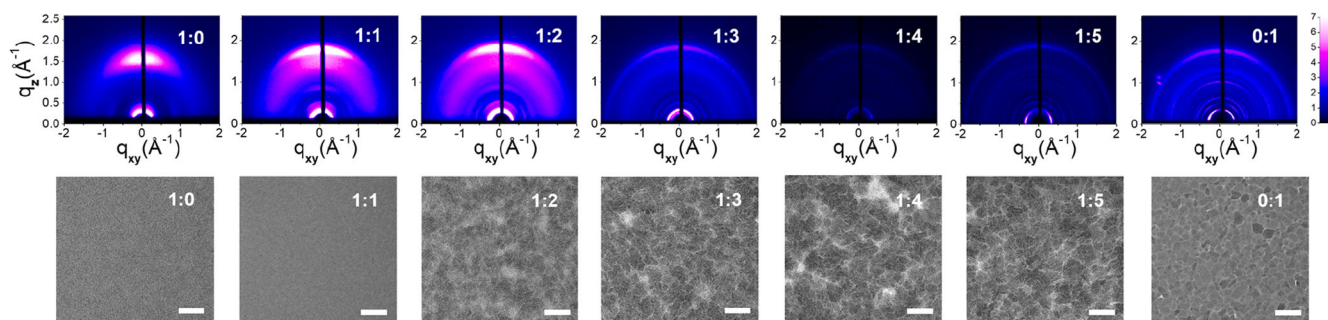


Fig. 3 Photovoltaic and optical properties of the TPVs. **a** Architecture and cross-section scanning electron microscope (SEM) image of the TPV devices (the scale bar is 100 nm). **b** J - V characteristics for TPV with AVT of 70.6% (D:A = 1:1.5, precursor concentration = 15.5 mg/mL), 75.6% (1:2, 15 mg/mL) and 80.4% (1:1.5, 9 mg/mL), respectively. Transmission (T), reflection (R) and external quantum efficiency (EQE) properties for the TPV devices with AVT of 70.6% (**c**) and 80.4% (**d**). **e** J - V curves for TPV with AVT of 80.5% from different illumination directions.

Table 2. Summarization of optical and photovoltaic parameters in TPVs with the AVT exceeding 70%.

PTB7-Th:IEICO-4F (D:A ratio, precursor concentration)	AVT (%)	CRI	V_{OC} (V)	J_{SC}/J_{EQE} (mA·cm ⁻²)	FF (%)	PCE (%)
1:1.5, 9 mg/mL	80.4	92.4	0.705	5.68/5.39	59.3	2.38
1:2, 15 mg/mL	75.6	90.0	0.697	7.87/7.31	63.0	3.46
1:1.5, 15.5 mg/mL	70.6	86.3	0.703	9.45/9.08	61.0	4.06

**Fig. 4** GIWAXS and TEM characterization of photovoltaic BHJ films prepared with various D–A ratios. The scale bar is 200 nm.

summarized in Supplementary Tables 6, 7 and plotted in Fig. 2a–c. The impact of D–A ratio and film precursor concentration on the transmission property of TPVs is essentially consistent with the related BHJ films. By adjusting the precursor condition, the AVT of TPVs can be tuned in the range of 40–85%. Similar to the BHJ films, the modeling results of TPVs clearly show the trend of AVTs changing with the precursor conditions of the active layers (Fig. 2c). In accordance with the results of modeling, the AVT of TPVs can be tuned more precisely.

The AVT of films and TPVs are listed and compared in Table 1. The results show that the AVT of TPVs is highly dependent on the AVT of photovoltaic films. It is only ~2% of fluctuation between the AVT of films and TPV devices (Supplementary Fig. 9). The high consistency of the transmission of the film and the device is chiefly attributed to the high transparency of substrate, transparent electrodes, and the charge selective layers. In addition, an interesting phenomenon is found that the AVT cannot be impacted a lot after the top transparent electrode is loaded, even if the transparent electrode itself is not completely transparent. Compared with the organic BHJ films, the TPVs show an improved CRI value when the film thickness is higher than 21 nm (Supplementary Fig. 10a–c and Supplementary Table 8). It is worthy to note that all the devices with AVT of over 70% show the CRI exceeding 85, which indicates that the high color reproduction capability of the highly transparent TPVs.

It is well known that the D–A ratio and active layer thickness can also essentially influence the photovoltaic performance of the device. The summarized results on device photovoltaic performance show that the device efficiency can be achieved 5.29%, 4.36%, 3.38%, and 1.61% for the TPV device with the AVT of 55.3%, 66.3%, 70.9%, and 80.5%, respectively (Table 1, and Supplementary Tables 9, 10). It should be mentioned that these PCE values are only the best results for the devices prepared under that certain precursor condition, and it cannot stand by the highest efficiency of the TPVs with the certain AVT values. Guide from the obtained results, the device performance for the TPVs with the AVT of > 70%, 75%, and 80% can be optimized with the PCE of 4.06%, 3.46%, and 2.38%, respectively (Fig. 3b and Table 2). The transmission (T), reflection (R), external quantum efficiency (EQE) curves are also plotted in Fig. 3c, d and Supplementary Figure 11 for the optical consistency check. Because of the double-side transparent electrodes, the TPVs can work and output the electric power when irradiating the light from both sides of the device. As

an example, the TPV device with the AVT of 80.5% irradiate from the ITO side shows higher efficiency than being irradiated from Ag NWs side (Fig. 3e and Supplementary Table 11). The EQE characterization confirms that the difference in the device performance mainly comes from the influence of photocurrent (Supplementary Figure 12).

Based on the obtained efficiencies of TPV devices, the PCEs and light utilization efficiencies ($LUE = PCE \times AVT$) are also plotted and modeled to reveal the relationship between device efficiency with the precursor condition of active layers (Fig. 2d–f and Supplementary Fig. 10d–f). The clear contour lines in the modeling images can precisely guide the preparation of the TPVs to match the requirements of the applications under various application environments. The parameters of AVT, PCE, and LUE collected from over 200 TPV devices are also plotted as the function from each other in Fig. 2g–i (the detailed parameters are organized in Supplementary Table 12). The comprehensive data can clearly show the optical performance changes from films to TPVs, and also accurately reflect the corresponding photovoltaic performance of the devices.

The D–A ratio not only affects the device transparency but also impacts the device performance. As showing in Supplementary Fig. 13, the EQE and internal quantum efficiency (IQE) degradation is believed the cause of the photocurrent loss and thereby affect the device efficiency when reducing the donor content. To further understand the effect of balancing the device transparency and efficiency by varying the D–A ratio, the grazing-incidence wide-angle x-ray scattering (GIWAXS), and transmission electron microscopy (TEM) characterization for the BHJ films are carried out (Fig. 4 and Supplementary Fig. 14). The GIWAXS results show that the BHJ film with D–A ratio of 1:2 presents the strongest intermolecular π - π stacking effect which indicates the efficient charge transportation from donor to acceptor³¹. The film with D–A ratio of 1:4 shows the weakest scattering signal and indicates the lowest molecular ordering. When the D–A ratio reaches 1:5, the BHJ film presents a similar behavior with the pure acceptor film, which suggests the poor charge transport efficiency between donor and acceptor. The TEM images exhibit that the BHJ film with D–A ratio of 1:2 presents the proper D–A blending morphology with the continuous charge transfer channel and without the obvious phase separation. When the D–A ratio is over 1:4, the phase separation becomes obvious which indicates the low charge-separation efficiency. The hole transfer channel

formed by the donor also gradually changes to discontinuous and then influences the charge transfer efficiency and finally impacts the device performance⁵.

It is worth noting that the D–A ratio can also influence the film thickness by influencing the precursor viscosity (Supplementary Table 4 and Supplementary Fig. 15). When the D–A ratio changes from 1:1 to 1:10, the film thickness changes from 101 nm to 42 nm for [20 mg/ml] set of films. Interestingly, we found that, regardless of the D–A ratio, when the film thickness is close to 115 nm, the film AVT will exceed 50%; when the film thickness is less than 100 nm, 70 nm, and 30 nm, the film AVT is expected to exceed 60%, 70%, and 80%, respectively. The summarized results indicate that the AVT of the BHJ films is strongly correlated with the film thickness and its changing trend strictly follows the absorption formula of semiconductor materials (Supplementary Figs. 16, 17). When the film thickness is fixed, the D–A ratios can only slightly influence the AVTs since the donor only has a little part of visible absorption. However, as investigated above, the D–A ratio is one of the key factors to affect the device photovoltaic performance since it can dramatically influence the film morphology and charge transport process. Thus, we can simply conclude that the film thickness plays a decisive role for the AVT in our TPVs, and both the D–A ratio and film thickness together affect the device efficiency (Supplementary Fig. 18). To date, the phenomena have not been observed in semitransparent organic solar cells yet, because the thicknesses of active layers are generally exceeding 100 nm in semitransparent organic solar cells and it is not sensitive to the D–A ratios in the thick films^{5,24,25}.

In addition, the photovoltaic performance drops sharply when the thickness of the active layer is lower than 30 nm. The devices worked poorly when the thickness is lower than 15 nm. Therefore, the upper limit of AVT for the PTB7-Th:ICFO-4F-based TPVs in this work is about 82%, and the approach of increasing the transparency by reducing the film thickness of the active layer will lose its practical significance when beyond this range. The result reveals the balance boundaries of device transparency and efficiency through changing the film thickness and the D–A ratio. And the study once again reflects the contradiction between transparency and efficiency on TPVs, and also the necessity of balancing these two parameters. The research is also expected to help the design of TPV applications by well-balancing transparency and efficiency.

Influence of the transparent electrode

Since the transparent top electrode is the second key factor for the TPVs, it has a vital impact on the optical and photovoltaic performance of the TPV devices. We introduced PH1000 as the transparent electrode to replace the AgNWs electrode to double-check our above observation. The inverted structure TPVs with PH1000 as the top transparent electrode show close results with the Ag NWs-based normal structure TPVs (Supplementary Fig.

19a). The results not only provide a good reference to strongly support the observations on Ag NWs-based TPVs but also indicate the light-harvesting BHJ layers decisive influence the TPV performance rather than the highly transparent electrode or the device structure in this study (Supplementary Figs. 19–24 and Supplementary Tables 13–21). Moreover, the study suggests that the transparencies of semitransparent solar cells are expected to be further improved by using the highly transparent electrode including Ag NWs and PH1000 to replace the thin-metal-film transparent electrodes^{6,24,25}.

TPV modules on rigid substrates

In accordance with the results of the above research, both optical and photovoltaic performance are encouraged and it exhibits the great potential of highly transparent TPVs on smart device applications with strict optical and power supply requirements²⁰. However, the devices with the square millimeters area are hard to be applied in our real-life due to the low output power including the limit voltage and low current density. The TPV devices with the larger output power are needed for exploring practical applications. Therefore, the TPV modules with device area up to 10 cm² are fabricated to verify its possibility as a power source for the other electrical devices in our following study.

By finely controlling the power of the laser source, three laser-patterning lines (P1, P2, and P3) can be successfully prepared for TPV modules, which is the key fabrication process for the TPV modules (Supplementary Fig. 25). The three-cell module with the device area of ~1 cm² and the eight-cell module with the device area of ~10 cm² in series-connection were prepared on the rigid glass/ITO substrates. Fig. 5a, b shows the *J–V* curves of the modules measured under AM 1.5 G simulated solar irradiance. For the three-cell modules with the AVT of ~70% and 80%, the device PCE achieved 2.93% and 1.37%, respectively (Supplementary Table 22). For the eight-cell modules with the AVT of ~70% and 80%, the device PCE is obtained of 2.31% and 1.12%, respectively (Supplementary Table 23). The efficiencies of large area TPV modules still keep at a high level compared with the small-area devices, which suggests the reliable preparation process and sufficient energy output of the modules.

Figure 5c shows the photograph of the large area TPV module. The device exhibits high visible transparency and the background of buildings, trees and clouds can be clearly seen through the TPV module, and the object colors remain very well. Since the transparency is comparable with double-glazed windows³², the TPV module with the fine photovoltaic performance is expected to be explored as the self-powered smart windows for buildings and vehicles (Supplementary Video 1). Considering the curtains may be used in actual applications to block the strong sunlight irradiation at noon, a piece of printer paper is put behind the TPV module to simulate the curtains for reflecting the irradiation light. With the diffuse reflection paper, the short-circuit current density

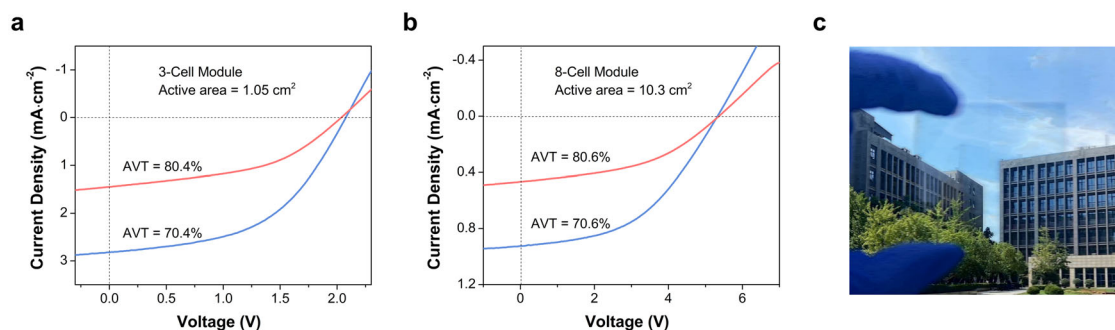


Fig. 5 Photovoltaic properties of the TPV module. *J–V* characteristics for TPV with active area of 1.05 cm² (a) and 10.3 cm² (b). c Photograph of TPV module with AVT of 80.6%.

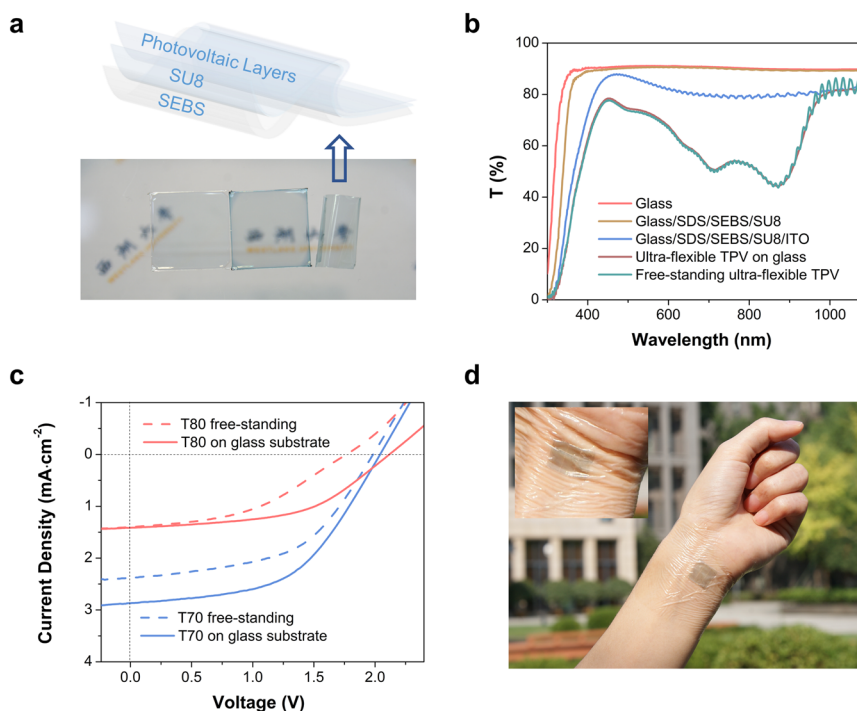


Fig. 6 Properties of the ultra-flexible TPV devices. **a** Architecture of the ultra-flexible TPV device. The bottom photograph shows the ultra-flexible substrate (left), ultra-flexible TPV devices on the glass substrate (middle), and the free-standing ultra-flexible TPV device (right), respectively. **b** Transmission properties for the substrate, film and device. **c** $J-V$ characteristics for ultra-flexible TPVs with AVT of $\sim 70\%$ (T70) and AVT of $\sim 80\%$ (T80) before and after peeled off from the glass substrate. **d** The ultra-flexible TPV device attached conformably to a human wrist (the inset shows the details of the ultra-flexible TPV device when bent the wrist).

(J_{SC}) of the TPV module with the AVT of 80.4% is increased around 50% and result in the enhancement of the device PCE from 1.37% to 1.90% (Supplementary Fig. 26 and Supplementary Table 24). Importantly, the output voltage of TPV modules can easily achieve over 5 V which is sufficient to charge the smart devices, such as smartphones, smartwatches, and some blue-tooth devices. The Supplementary Video 2 demonstrate the smartphone charging process by the TPV modules. The instance also illustrates the application potential of TPV modules as the car windows to drive the low-power electronic devices.

TPV modules on ultra-flexible substrates

Ease of processing on the flexible substrate is one of the advantages of organic semiconductors. With the improvement of the device efficiency, some OPVs are fabricated on ultra-flexible and stretchable substrates to act as the power source for soft robots, electronic skin, and photonic skin in recent years^{33–35}. The prospective studies explored a feasible way to utilize the OPVs on wearable smart devices^{35,36}. With the high efficiency and invisible property, the TPV modules can not only provide robust output power but also meet the strict aesthetic requirements for wearable devices. Aiming to explore the broader application chance for the TPV modules, we further attempted to fabricate the TPV module on the ultra-flexible substrate in this work (Fig. 6).

The ultra-flexible TPVs with ultra-flexible substrate need to be prepared on the rigid glass substrate and finally peeled off from the rigid substrate to complete the fabrication process. A thin sodium dodecyl sulfate (SDS) layer is introduced as the sacrificial layer to help the peel-off process of the obtained ultra-flexible devices. It is worthy to note that the sacrificial layer is crucial not only for the separation process but also for the performance of ultra-flexible devices. The thin SEBS layer ($\sim 5 \mu\text{m}$) is worked as the flexible substrate and the SU-8 layer ($\sim 1 \mu\text{m}$) is used to form a smooth surface of the ultra-flexible TPVs (Fig. 6a). Since the

thickness of the active layer is only 20–70 nm, the smoothness of the substrate is one of the key factors which can greatly influence the efficiency of devices. The sputtered ITO layer is adopted as the transparent bottom electrode. The three-cell modules are fabricated with the ultra-flexible substrate by carefully controlling the laser-etching conditions, and the additional fabrication processes are similar to the rigid TPV modules.

The bottom image in Fig. 6a shows the photograph of the glass/SDS/SEBS/SU-8 substrate (left), flexible TPV devices on the glass substrate (middle), and the free-standing ultra-flexible TPV device (right), respectively. All samples display high transparency and the logo of the Westlake University can be seen very clearly through the samples. The free-standing ultra-flexible TPV device (without pattern lines) presents a natural curled state which indicates the well flexibility of the device. After being peeled off from the rigid glass substrate, the transmission spectrum of the free-standing ultra-flexible device only shows a little change from it with glass substrate (Fig. 6b), which results in the AVT changing from 70.8% to 70.0% (Supplementary Table 25). Since the thickness of the whole device is only a few micrometers, the TPV devices exhibit naturally ultra-flexible and ultra-lightweight properties. For example, it is easy to curl as the tube and attracted by the static electricity (Supplementary Video 3). The fresh prepared ultra-flexible devices are suggested to be operated and transferred as early as possible before it curled.

The $J-V$ characterization is also carried out for the ultra-flexible TPV modules (Fig. 6c). The device before being peeled from the glass substrate exhibits an open-circuit voltage (V_{OC}) of 2.04 V, a J_{SC} of 2.87 mA cm^{-2} , and a fill factor (FF) of 52.0%, and resulting in a PCE of 3.04%. Correspondingly, the free-standing ultra-flexible device exhibits an efficiency of 2.44% (Supplementary Table 26). The efficiency drop is mainly caused by the drop of J_{SC} , which implies that the separation process affects the performance of the ultra-flexible device. The more stable and flexible transparent electrodes are expected to be developed to replace the

conventional rigid ITO electrode. However, the limited efficiency loss is acceptable for the ultra-flexible device. With the significant advantages of ultra-flexible and ultra-lightweight, the highly transparent TPV modules offer enormous application potential in the flexible electronics field (Fig. 6d).

In addition to the optical and photovoltaic properties of the TPV device, the stability of the device is also considered since stability is crucial for the applications. The rigid devices and ultra-flexible devices with AVT ~80% are used to preliminarily evaluate the stability (Supplementary Fig. 27). Related devices are stored in the glovebox without encapsulation for two weeks, and the efficiencies show a slight drop in the first week. However, the degradation of the devices becomes slow after 10 days test and the efficiencies maintain over 80% of the initial for all devices when the test is stopped. The fine stability of the devices implies the good potential of our TPVs to be applied in the various applications.

Photovoltaic is an important mode to utilize renewable clean solar energy which presents an effective way to solve the energy problems and environmental problems in this century³⁷. As an essential supplement, the TPVs offers a good choice to overcome the limitations of opaque photovoltaics, and it can be placed at the high human activity areas such as the windows of offices, living rooms, and landscape exterior walls, etc. In this study, by taking the reported organic semiconductors as an example, we demonstrate that how to balance the efficiency and transparency in TPVs. The interrelationships of optical transmission and photovoltaic properties for the photovoltaic films and TPVs are systematically studied. The results reveal that the film thickness plays a decisive role in the TPV transparency, and both the D–A ratio and film thickness together affect the device photovoltaic performance. The systematical studies are helping to precisely guide the preparation of the TPVs with expected AVT of from 40% to over 80%. The device efficiency can achieve as high as 4.06% and 2.38% when the AVT is exceeding 70% and 80%, respectively.

The large area TPV modules are also successfully prepared. The development of the TPV modules with high optical transparency and photovoltaic performance enables more area of building surface and vehicle windows to be used to generate electricity without impacting the aesthetics, and it also presents a practical option for designing the building-integrated photovoltaic (BIPV) and self-power windows^{20,38}. In addition, the highly transparent TPV modules are also attempted to prepare and test on the ultra-flexible substrates in our study. The milliwatt-level power output and invisible property indicate the flexible TPV modules are a good choice for the power supply source of wearable smart devices such as electronic skin and photonic skin.

The high AVT and PCE make our TPV devices one of the best performing TPVs reported to date (Supplementary Fig. 28 and Supplementary Table 27). The initial demonstration of ultra-flexible TPV reveals that the reported TPVs are not only a powerful supplement to opaque photovoltaics for electricity generation but also a promising candidate for the power supply source of wearable electronic devices. This work provides a good instance to utilize the reported organic-based semiconductors to produce the highly efficient TPVs which can perfectly meet the critically high level of aesthetics requirements for actual applications, and importantly, it exhibits a basic reference to balance the transparency and efficiency of the TPVs. In future research, exploring the semiconductors with invisible-light-harvesting ability is still the most effective strategy for the development of the TPVs, and adjusting the film thickness and D–A ratio are also the effective complemented approaches to further balance the device optical and photovoltaic performance.

METHODS

Materials

ITO substrate (~30 nm, ~70 Ω sq⁻¹, Guangzhou Shenghua Tech. Inc.), PEDOT (Clevios P VP.Al 4083, Heraeus), PTB7-Th (Organtec Ltd.), IEICO-4F (Organtec Ltd.), Zinc acetate dihydrate (99%, bidepharm.), MoO₃ (99.9995%, Alfa Aesar), Ag NWs (5 mg/mL in ethanol, average length of ~30 μ m, diameter of ~40 nm, J&K), PH1000 (Clevios PH1000, Heraeus), SDS (10% SDS solution, Sangon Biotech), SEBS (H1062, AsahiKASEI), SU-8 (SU-8 2005, MicroChem), Polydimethylsiloxane (PDMS) (Sylgard 184) base and curing agent (Dow Corning). ZnO nanoparticles was prepared by the reference method³⁹.

Device Fabrication

To prepare the small-area TPV devices (Glass/ITO/PEDOT/PTB7-Th:IEICO-4F/ZnO/Ag NWs), the following steps were used. The ITO substrate was ultrasonically cleaned with surfactants, deionized water and isopropanol in sequence. PEDOT (diluted to 50% by water for use) was spin-coated on the ITO at 4000 rpm for 25 s, and then annealed at 120 °C for 10 min. PTB7-Th and IEICO-4F were dissolved in chlorobenzene with 4% CN additive, and spin-coated on the PEDOT layer at 2000 rpm for 60 s, annealing at 100 °C for 10 min. By changing the ratio of donor and acceptor and the total concentration of the active layer solution, to obtain the active light-absorbing layer with different thicknesses. The ZnO nanoparticles was then spin-coated on the active layer to form the electron transport layer. Next, Ag NWs were spin-coated on the ZnO layer at 2000 rpm for 50 s to form the top transparent electrode. The pulsed laser was used to pattern and etch the Ag NWs layer to determine the active area of 5 mm². (The pulsed laser WL-30W produced by Liaocheng Weilan Laser Equipment Co., Ltd. The laser power is 4.5 W, and the etching speed is 1000 mm/s with the laser frequency of 80 kHz. The frequencies are slightly changed to get a suitable etching depth of the layered film. The etching lines would go deeper with lower frequencies).

To fabricate TPV modules on the glass substrates (Glass/ITO/PEDOT/PTB7-Th:IEICO-4F/ZnO/Ag NWs), the following steps were used. For the devices with active area of ~1 cm² and 10 cm², the preparation of each layer is the same as the small-area device described above. It should be noted that the ITO, ZnO and Ag NWs layers need to be patterned and etched by pulsed laser to complete the series design of the device. For the ITO layer (P1), the etching speed was 400 mm/s, laser power was 10.5 W and frequency is 20 kHz. After depositing the PEDOT/PTB7-Th:IEICO-4F/ZnO multiple layers, the P2 line was prepared by laser etching with the laser power of 4.5 W, etching speed of 1000 mm/s, and the laser frequency of 20 kHz. After the Ag NWs deposited, laser etching was continued with the laser power of 6 W, etching speed of 1000 mm/s, and the laser frequency of 80 kHz to form the P3 line and complete the fabrication of the module devices.

To prepare the small-area TPV devices with PH1000 as the transparent electrode (Glass/ITO/ZnO/PTB7-Th:IEICO-4F/MoO₃/PH1000), we used the following steps. Preparation of the ITO, ZnO and active layer was consistent with the above method. After finishing the active layer, the substrate was transferred into the evaporation chamber to deposit the MoO₃ layer with 10 nm. For the PH1000 transparent electrode, lamination method was used according to the reference reports⁴⁰. PH1000 was spin-coated on the PDMS substrates at 4000 rpm for 40 s, after drying in the air about 3 min, PDMS was then laminated on the MoO₃ layer and peeled off after a while, and then the TPV device was successfully fabricated. The device area of ~4 mm² was determined by the overlap area of ITO and PH1000 electrodes.

To prepare the ultra-flexible TPV devices (SEBS/SU-8/ITO/PEDOT/PTB7-Th:IEICO-4F/ZnO/Ag NWs), the following steps were adopted. The ultra-flexible TPVs need to prepare on the rigid glass substrate, and then peel off from the glass substrate to obtain the final free-standing ultra-flexible TPV devices. The ultra-flexible transparent substrate was firstly prepared on the rigid glass substrate. Sodium dodecyl sulfate (SDS) of 1% concentration in DI water was spin-coated at 4000 rpm on glass substrate as the sacrificial layer. Ultra-flexible transparent substrate of SEBS (~5 μ m)/SU-8 (~1 μ m) was then prepared on the SDS layer. The SEBS layer and the SU-8 layer was subsequently spin-coated at 1500 rpm for 30 s and 2000 rpm for 30 s, respectively. The substrate was then exposed in UV light to get solidified. ITO of 180 nm in thickness was sputtered on the SU-8 layer with metal mask to form the bottom transparent electrodes. P2 and P3 lines of the serial TPV devices were then prepared in the same way as the 3-cell module devices on rigid substrate. The pulsed laser with the power of 0.3 W, etching speed of 1000 mm/s, frequency of 55 kHz (P2) and 80 kHz (P3) was used to draw the pattern lines of the devices. The whole device on

SEBS/SU-8 substrate was finally mechanically separated from the glass substrate to finish the ultra-flexible TPV device. The area of ultra-flexible 3-cell module device is 0.64 cm².

Film and device characterizations

Transmission and reflection spectra of films and devices were measured by UV–Vis–NIR spectrophotometer (Cary 6000i). The thickness of films was determined by Stylus Profiler (P7). Morphologies of films and devices were characterized by field emission scanning electron microscope (SEM, Hitachi, Regulus 8230) and high-resolution transmission electron microscope (TEM, Thermo Fisher Scientific, Talos F200X G2). Grazing-incidence wide-angle X-ray scattering (GIWAXS) was performed with DUO micro-sourced single-crystal X-ray diffractometer (Bruker, D8 Venture). The X-ray wavelength was 1.54184 Å. The sample to detector distance was about 70 mm. For the photovoltaic properties, current density–voltage (*J*–*V*) curves were obtained with the Keithley 2400 source, under the simulated AM 1.5 G illumination by 450 W Xenon-lamp (Newport, M94043A). The light intensity was calibrated by the certified Si solar cell (xenon arc lamp with the spectral-mismatch factor of 1.06 for the devices studied). Devices were scanned at a rate of 50 mV/s with dwell time of 30 ms. The device active area was measured by the Optical microscope (SDTOP CX40M). Additionally, EQE was collected by Newport Quant X-300. The light intensity was also calibrated by the certified Si detector.

Model Fitting

The contour-color fill function of Origin 2021 was used for model-fitting. Taking Fig. 1e as an example, the total concentration values of active layer precursors (25, 20, 15, 10, 5) and the *x* values of 1:*x* in the D–A ratio (1, 2, 3, 4, 5, 10) were used as X and Y coordinates respectively. The corresponding film AVT values was used as Z coordinate, and there were 30 sets of data points in total. The data points were plotted using contour-color fill function. In order to make the image more intuitive, fill the AVT values with the same color in a relatively close range. For example, fill the AVT values with the same color between 40 and 45%.

Theoretical AVT calculation

The theoretical AVT of the active layer was calculated with the light propagation equation in a semiconductive isotropic medium, which is deduced from Maxwell's equations,

$$I = I_0 \exp(-a * x) \quad (1)$$

where *I* is the light intensity when it propagates a distance of *x* in the *x* direction; *I*₀ is the intensity of the incident light; *a* is the wavelength related absorption coefficient. Taking the reflection from the two interfaces into consideration, the transmission coefficient can be expressed as,

$$T = \frac{I}{I_0} = (1 - R)^2 \exp(-a * x) \quad (2)$$

an empirical value of ~8% light loss from reflection was applied in the calculation. And then AVT can be calculated as,

$$AVT_{cal} = \frac{I}{I_0} = 0.92 * \frac{\int E(\lambda) I_0(\lambda) \exp[-\alpha(\lambda) * x] d\lambda}{\int E(\lambda) I_0(\lambda) d\lambda} \quad (3)$$

where *E*(λ) represents human eye photonic response and *x* is equal to the film thickness, the integrated wavelength range is 430–670 nm.

DATA AVAILABILITY

The data that support the findings of this study are available from the corresponding author upon reasonable request.

Received: 21 January 2022; Accepted: 10 May 2022;

Published online: 07 June 2022

REFERENCES

- Chang, S.-Y., Cheng, P., Li, G. & Yang, Y. Transparent polymer photovoltaics for solar energy harvesting and beyond. *Joule* **2**, 1039–1054 (2018).
- Traverse, C. J., Pandey, R., Barr, M. C. & Lunt, R. R. Emergence of highly transparent photovoltaics for distributed applications. *Nat. Energy* **2**, 849–860 (2017).
- Li, M. Z. et al. Vacuum-deposited transparent organic photovoltaics for efficiently harvesting selective ultraviolet and near-infrared solar energy. *Sol. RRL* **5**, 2000564 (2020).
- Liu, Q. et al. Light harvesting at oblique incidence decoupled from transmission in organic solar cells exhibiting 9.8% efficiency and 50% visible light transparency. *Adv. Energy Mater.* **10**, 1904196 (2020).
- Zuo, L., Shi, X., Fu, W. & Jen, A. K. Y. Highly efficient semitransparent solar cells with selective absorption and tandem architecture. *Adv. Mater.* **31**, 1901683 (2019).
- Liu, Y. et al. Unraveling sunlight by transparent organic semiconductors toward photovoltaic and photosynthesis. *ACS Nano* **13**, 1071–1077 (2019).
- Liu, D., Yang, C. & Lunt, R. R. Halide perovskites for selective ultraviolet-harvesting transparent photovoltaics. *Joule* **2**, 1827–1837 (2018).
- Liu, D. et al. Lead halide ultraviolet-harvesting transparent photovoltaics with an efficiency exceeding 1%. *ACS Appl. Energy Mater.* **2**, 3972–3978 (2019).
- Lopez-García, A. J. et al. UV-selective optically transparent Zn(O,S)-based solar cells. *Sol. RRL* **4**, 2000470 (2020).
- Davy, N. C. et al. Pairing of near-ultraviolet solar cells with electrochromic windows for smart management of the solar spectrum. *Nat. Energy* **2**, 17104 (2017).
- Lunt, R. R. Theoretical limits for visibly transparent photovoltaics. *Appl. Phys. Lett.* **101**, 043902 (2012).
- Naim, W. et al. Transparent and colorless dye-sensitized solar cells exceeding 75% average visible transmittance. *JACS Au* **1**, 409–426 (2021).
- Véron, A. C. et al. NIR-absorbing heptamethine dyes with tailor-made counterions for application in light to energy conversion. *Org. Lett.* **16**, 1044–1047 (2014).
- Lunt, R. R. & Bulovic, V. Transparent, near-infrared organic photovoltaic solar cells for window and energy-scavenging applications. *Appl. Phys. Lett.* **98**, 113305 (2011).
- Yan, C. et al. Non-fullerene acceptors for organic solar cells. *Nat. Rev. Mater.* **3**, 18003 (2018).
- Xie, Y. et al. Highly transparent organic solar cells with all-near-infrared photo-active materials. *Small Methods* **3**, 1900424 (2019).
- Xia, R., Brabec, C. J., Yip, H.-L. & Cao, Y. High-throughput optical screening for efficient semitransparent organic solar cells. *Joule* **3**, 2241–2254 (2019).
- Li, Y. et al. High efficiency near-infrared and semitransparent non-fullerene acceptor organic photovoltaic cells. *J. Am. Chem. Soc.* **139**, 17114–17119 (2017).
- Brus, V. V. et al. Solution-processed semitransparent organic photovoltaics: from molecular design to device performance. *Adv. Mater.* **31**, 1900904 (2019).
- Wang, D. et al. High-performance and eco-friendly semitransparent organic solar cells for greenhouse applications. *Joule* **5**, 945–957 (2021).
- Yuan, J. et al. Single-junction organic solar cell with over 15% efficiency using fused-ring acceptor with electron-deficient core. *Joule* **3**, 1140–1151 (2019).
- Hu, Z., Wang, Z., An, Q. & Zhang, F. Semitransparent polymer solar cells with 12.37% efficiency and 18.6% average visible transmittance. *Sci. Bull.* **65**, 131–137 (2020).
- Song, X. et al. Controlling blend morphology for ultrahigh current density in nonfullerene acceptor-based organic solar cells. *ACS Energy Lett.* **3**, 669–676 (2018).
- Hu, Z., Wang, Z. & Zhang, F. Semitransparent polymer solar cells with 9.06% efficiency and 27.1% average visible transmittance obtained by employing a smart strategy. *J. Mater. Chem. A* **7**, 7025–7032 (2019).
- Xu, C. et al. Wide bandgap polymer with narrow photon harvesting in visible light range enables efficient semitransparent organic photovoltaics. *Adv. Funct. Mater.* **31**, 2107934 (2021).
- Yao, H. et al. Design, synthesis, and photovoltaic characterization of a small molecular acceptor with an ultra-narrow band gap. *Angew. Chem. Int. Ed.* **56**, 3045–3049 (2017).
- Liao, S. H., Jhuo, H. J., Cheng, Y. S. & Chen, S. A. Fullerene derivative-doped zinc oxide nanofilm as the cathode of inverted polymer solar cells with low-bandgap polymer (PTB7-Th) for high performance. *Adv. Mater.* **25**, 4766–4771 (2013).
- Guo, F. et al. Nanowire interconnects for printed large-area semitransparent organic photovoltaic modules. *Adv. Energy Mater.* **5**, 1401779 (2015).
- Fan, X. Doping and design of flexible transparent electrodes for high-performance flexible organic solar cells: recent advances and perspectives. *Adv. Funct. Mater.* **31**, 2009399 (2020).
- Zhou, Y. et al. All-plastic solar cells with a high photovoltaic dynamic range. *J. Mater. Chem. A* **2**, 3492–3497 (2014).
- Chen, M. et al. Influences of non-fullerene acceptor fluorination on three-dimensional morphology and photovoltaic properties of organic solar cells. *ACS Appl. Mater. Interfaces* **11**, 26194–26203 (2019).
- Ghosh, A., Selvaraj, P., Sundaram, S. & Mallick, T. K. The colour rendering index and correlated colour temperature of dye-sensitized solar cell for adaptive glazing application. *Sol. Energy* **163**, 537–544 (2018).
- Bauer, S. et al. 25th anniversary article: a soft future: from robots and sensor skin to energy harvesters. *Adv. Mater.* **26**, 149–161 (2014).

34. Wang, S. et al. Skin electronics from scalable fabrication of an intrinsically stretchable transistor array. *Nature* **555**, 83–88 (2018).
35. Jinno, H. et al. Self-powered ultraflexible photonic skin for continuous bio-signal detection via air-operation-stable polymer light-emitting diodes. *Nat. Commun.* **12**, 2234 (2021).
36. Park, S. et al. Self-powered ultra-flexible electronics via nano-grating-patterned organic photovoltaics. *Nature* **561**, 516–521 (2018).
37. Green, M. A. How did solar cells get so cheap? *Joule* **3**, 631–633 (2019).
38. Li, Z., Ma, T., Yang, H., Lu, L. & Wang, R. Transparent and colored solar photovoltaics for building integration. *Sol. RRL* **5**, 2000614 (2021).
39. Liu, D. & Kelly, T. L. Perovskite solar cells with a planar heterojunction structure prepared using room-temperature solution processing techniques. *Nat. Photonics* **8**, 133–138 (2013).
40. Gupta, D., Wienk, M. M. & Janssen, R. A. J. Efficient polymer solar cells on opaque substrates with a laminated PEDOT:PSS top electrode. *Adv. Energy Mater.* **3**, 782–787 (2013).

ACKNOWLEDGEMENTS

The authors thank for the facility support and technical assistance from the Instrumentation and Service Center for Physical Sciences (ISCPs), as well as from the Center for Micro/Nano Fabrication at Westlake University. We also appreciate the talent work on the GIWAXS data collection from Dr. Xiaohu Miao in ISCPs at Westlake University. This study was supported by the Westlake Education Foundation.

AUTHOR CONTRIBUTIONS

D.L. conceived the project and directed the study. R.M. and Q.J. carried out the device fabrication on rigid substrate and performance measurements. Q.J. performed the GIWAXS and TEM characterization and treated the data. Q.J. also prepared the ultra-flexible modules and tested the performance. D.L. prepared the manuscript. All authors contributed to the data analysis and manuscript revisions.

COMPETING INTERESTS

R.M., Q.J., and D.L. have filed two patent applications based on the work in this manuscript.

ADDITIONAL INFORMATION

Supplementary information The online version contains supplementary material available at <https://doi.org/10.1038/s41528-022-00173-9>.

Correspondence and requests for materials should be addressed to Qianqing Jiang or Dianyi Liu.

Reprints and permission information is available at <http://www.nature.com/reprints>

Publisher's note Springer Nature remains neutral with regard to jurisdictional claims in published maps and institutional affiliations.



Open Access This article is licensed under a Creative Commons Attribution 4.0 International License, which permits use, sharing, adaptation, distribution and reproduction in any medium or format, as long as you give appropriate credit to the original author(s) and the source, provide a link to the Creative Commons license, and indicate if changes were made. The images or other third party material in this article are included in the article's Creative Commons license, unless indicated otherwise in a credit line to the material. If material is not included in the article's Creative Commons license and your intended use is not permitted by statutory regulation or exceeds the permitted use, you will need to obtain permission directly from the copyright holder. To view a copy of this license, visit <http://creativecommons.org/licenses/by/4.0/>.

© The Author(s) 2022